Available online at www.sciencedirect.com
ScienceDirect
Journal of Electron Spectroscopy and Related Phenomena 161 (2007) 43–50
JOURNAL OF ELECTRON SPECTROSCOPY and Related Phenomena
www.elsevier.com/locate/elspec

Progress on electron momentum spectroscopy studies at Tsinghua University in Beijing

J.K. Deng *, C.G. Ning, X.G. Ren, G.L. Su, S.F. Zhang, Y.R. Huang, T.C. Yang, K. Liu

Department of Physics and Key Laboratory of Atomic and Molecular NanoSciences of MOE, Tsinghua University, Beijing 100084, PR China

Available online 12 April 2007

Abstract

We report the new developments of electron momentum spectroscopy (EMS) studies at Tsinghua University in Beijing. A high sensitivity and high resolution (e, 2e) electron momentum spectrometer with simultaneous detection in energy and momentum was constructed recently. The EMS studies of distorted wave effects and chemical shift of core orbitals in molecules are presented in this paper.

Keywords: (e, 2e) Spectrometer; Distorted wave effects; Chemical shift; Core orbitals

1. Introduction

Electron momentum spectroscopy (EMS), based on a binary (e, 2e) ionization reaction, has been used to investigate the electronic structure of atoms, molecules, biomolecules and condensed matter [1–3]. Within the plane wave impulse approximation (PWIA), the target Hartree–Fock approximation (THFA) or target Kohn–Sham approximation (TKSA) and some other approximations [1], the measured (e, 2e) cross-section is proportional to the spherically averaged momentum distribution of a specific orbital. Therefore, EMS has the ability to provide direct experimental information on electronic structure and electron correlation dynamics. Moreover, it is worth noting from a chemical standpoint that EMS provides direct information on the binding energies, the behavior of electrons and the electron density in the chemically reactive individual outer valence orbitals, and molecule recognition [4].

However, most EMS studies have been limited to the valence orbitals of relatively small and stable molecules with impact energy of 1200 eV. Large molecules and chemical interesting low density targets such as free radicals, ions and van der Waals molecules and core orbitals of molecules are effectively beyond the reach of existing conventional instruments due to the limitations in sensitivity and resolution, caused by the fact that EMS is a coincidence counting experiment and also that a very large proportion of the available signal is wasted due to limitations in the angular and energy ranges. As a result of these limitations, many new types of experiments are unfeasible within a practical period of time with the existing spectrometers, and their realizations require major improvement in the sensitivity of EMS. In addition, the possibility to vary the experimental impact energy in EMS has both practical and theoretical significance. For instance, it might provide a validation of the PWIA and an estimation of the distorted wave effects [5], so to establish criteria for the application of the PWIA. To meet these requirements, a high sensitivity and high resolution (e, 2e) electron momentum spectrometer with simultaneous detections in energy and momentum was constructed in our laboratory recently [6]. Another feature of this spectrometer is that the impact energies can be varied from 400 eV to 2400 eV. With the new spectrometer we studied the distorted wave effects in molecules with the varied impact energies [5,7,8] and the core orbitals [9] characterized by very low (e, 2e) cross-section. In this paper, we present the structure and performance of the new spectrometer and the EMS investigation of the distorted wave effects in the ionization process and chemical shift of the core orbitals in molecules.

2. Electron momentum spectrometer

Fig. 1 presents cross-section of the set-up containing the symmetry axis of the instrument, which consists of an electron gun, a collision chamber, a four-element conical decelerating lens with two conical apertures at the first and fourth electrode, the double toroidal analyzer (DTA) and a pair of position sensitive detectors (PSDs) [6]. A homemade electron gun equipped with a

* Corresponding author. Tel.: +86 10 6278 5594.
E-mail address: djk-dmp@tsinghua.edu.cn (J.K. Deng).

0368-2048/$ – see front matter © 2007 Elsevier B.V. All rights reserved.
doi:10.1016/j.elspec.2007.04.001

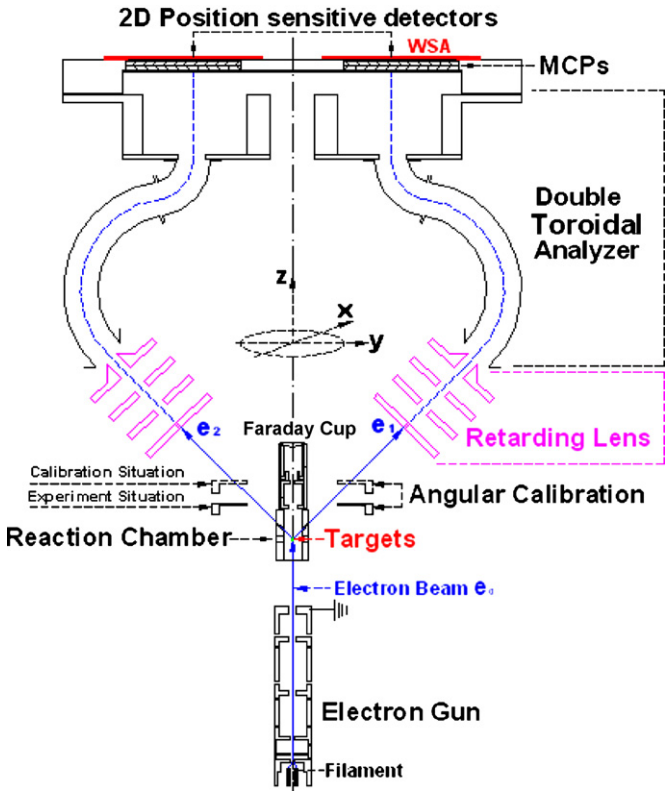

Fig. 1. Scheme of the high sensitivity and high resolution (e, 2e) electron momentum spectrometer at Tsinghua University.

heated thoriated tungsten filament provides the electron source. The electron beam is directed into a Faraday cup after passing through the collision chamber. Typically a current of about 2 μA is collected on the Faraday cup, which consists of an inner cup of 1 mm diameter and an outer cup. The gas jet is a nozzle of 0.5 mm diameter, which is directed toward the scattering point to form the intense target densities. Electrons leaving the (e, 2e) collision region along the conical surface at polar angle 45° are collimated with the two apertures. Both of the apertures are used to select only electrons at typically $\theta = 45 \pm 0.7°$. The two angle-selected electrons equally share the available energy ($E_1 \approx E_2$) and are decelerated by the conical lenses in order to achieve higher energy resolution. The performances in terms of resolution in energy, θ and ϕ angles have been considered simultaneously in the design of the DTA analyzer. The energy-analyzed electrons are detected by two wedge strip anode (WSA) PSDs placed behind the DTA exit aperture. Each detector covers the azimuthal angle range from −19° to +19°, so the measured coincident ϕ angle range is from −38° to +38°.

A digital multi-parameter coincidence measurement system based on universal serial bus (USB) interface was used for data acquisition in the (e, 2e) spectrometer. The details of the data acquisition system have been reported elsewhere [10]. Briefly, two WSA PSDs were used to detect the electrons. The fast timing signals are picked up via a decoupling capacitor and resistor attached to the exit surface of the micro-channel plates (MCPs) in the chevron pair. Two fast preamplifiers are used near the vacuum chamber to invert the timing signal from MCPs. The pulses from preamplifiers, which are amplified by fast amplifiers, pass through the constant fraction discriminations (CFD) to minimize the timing jitter. The fast pulses in nuclear instrument module (NIM) logic from one CFD are used as the start signal for time-to-amplitude conversion (TAC), and the signal from other CFD, after a suitable delay, as the stop signal. The amplitude of the output from TAC is proportional to the time difference between the start and the stop pulses. The charge hit on WSA is collected, respectively, from the three electrodes by charge sensitive preamplifiers, then amplified and shaped by spectroscopy amplifiers. These pulses are rather slow, but give a good signal to noise ratio. The signals are processed by the multi-parameters system, and transferred to a computer by the USB interface. To realize the USB 1.0 protocol, a microcontroller unit (MCU) and a USB interface chip were used. MCU was also used to control the system bus, and to realize the energy scan and other controls. Since MCU is programmable and directly orients the hardware, it is very flexible to realize these versatile controls with MCU. The on-line raw data are recorded on the computer hard disk, and the detailed information related to coincidence time spectra, binding energy spectra and electron momentum spectra can be obtained from the acquired raw data.

The details of the performance of the new spectrometer can be found in Ref. [6]. The typical energy resolution of the spectrometer is 0.8 eV at 50 eV passing energy, and 1.2 eV at 100 eV passing energy. The angular resolution is $\Delta\theta \approx \pm 0.7°$ and $\Delta\phi \approx \pm 1.9°$. It should be also noted that the counting rate has increased about 100 times compared to the former conventional spectrometer [11] in our lab. In order to give a straight insight of the performance of the new spectrometer, the electron density distributions of argon 3p and 3s, as well as 3s satellite states, are shown in Fig. 2. The inset in Fig. 2 is the binding energy spectrum summed over all ϕ angles, which can be well reproduced by Gaussian functions with 1.2 eV FWHM. Another feature of the spectrometer is that the impact energies can be

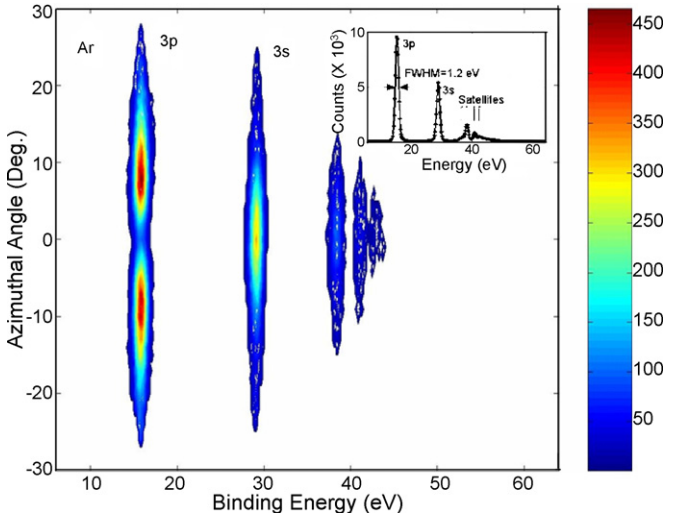

Fig. 2. Experimental electron density distribution of argon obtained under the impact energy 1000 eV and 100 eV pass energy. The inset shows the binding energy spectrum obtained by summing up the intensities along the azimuthal angle in the contour map. The energy resolution is 1.2 eV FWHM.

varied over a large range from 400 eV to 2400 eV. By using the widely adjustable impact energy, we have systemically explored some effects which exhibit a strong impact energy dependence [5,7,8,12–16], and by using the high collection efficiency, we have investigated the ionization with excitation of helium [17] and the chemical shift of core orbital [9]. Moreover, we have also studied valence orbitals of several molecules [18–22] with much higher statistical accuracy than our previous spectrometer [11].

3. Distorted wave effects of molecules

In the (e, 2e) reaction of EMS, the collisions and interactions can be accounted for by using several approximations [1], such as PWIA, which requires that the incoming and outgoing electron energies have to be large enough to describe all the electrons by plane waves and large momentum transfer must be achieved so that the momentum and energy transferred to the target are absorbed by the ejected electron. The distorted wave approximations methods, for instance the distorted wave Born approximation (DWBA) or the distorted wave impulse approximation (DWIA), allow for the influence (distortion) on the incoming and outgoing electron waves due to interaction with the target and the ion, respectively. According to previous EMS measurements [1–3] the PWIA is adequate to describe the experimental results on atoms and molecules at the momentum (p) region below 1.0 a.u. Some discrepancies between PWIA calculations and EMS measurements in the high momentum region may be well understood by the distorted wave effects [1,13], since high momenta involve collisions near to the nucleus and thus imply significant penetration of the incoming and outgoing electrons wave functions in the region of r small.

The experimental electron momentum distributions of $1b_{3u}$ orbital of C_2H_4 [13], which is p-like and could be clearly resolved in the EMS binding energy spectra, measured at several incident energies (400–2400 eV) and the theoretical calculations are shown in Fig. 3. The theoretical orbital electron momentum distributions are calculated by density functional theory (DFT) and Hartree–Fock (HF) methods with 6-311++G** and 6-31G basis sets in the PWIA model. To compare the calculated cross-sections with experimental electron momentum profiles, we incorporated the effects of the finite acceptance angles of the spectrometer in both θ and ϕ in calculations with the method described in Ref. [23]. By comparing the experimental and theoretical momentum distributions of the orbital with different impact energies, we could find that the experimental data can be well described by the PWIA theoretical calculations in the lower momentum region over a wide range of impact energies. The theoretical calculations using DFT hybrid Becke–Perdew-3-parameters-Lee–Yang–Parr (B3LYP) functional with basis sets 6-311++G** can provide an excellent description of the experimental measurements, which indicates that the inclusion of electron correlation effects method with the saturated diffuse and polarization basis set calculation is essential for description of the highest occupied molecular orbital (HOMO) of ethylene in the chemically important larger r (lower p) region. Moreover, in the high momentum region some discrepancies are clearly observed, which are mainly due to distorted wave effects [1,13] since the distortion of plane waves becomes significant in the region of high momentum components of the bound electron wave function, close to the nucleus where the distorting potential is larger. In order to make this clearer, the difference between the experimental and PWIA cross-section, integrated over the momentum region 1.0 a.u. $< p <$ 1.6 a.u., were plotted as a function of the impact energy in Fig. 4. The PWIA calculations were performed using the B3LYP/6-311++G** basis set. It can be seen that the discrepancies in the cross-section become smaller when the impact energies are increased, which means that the

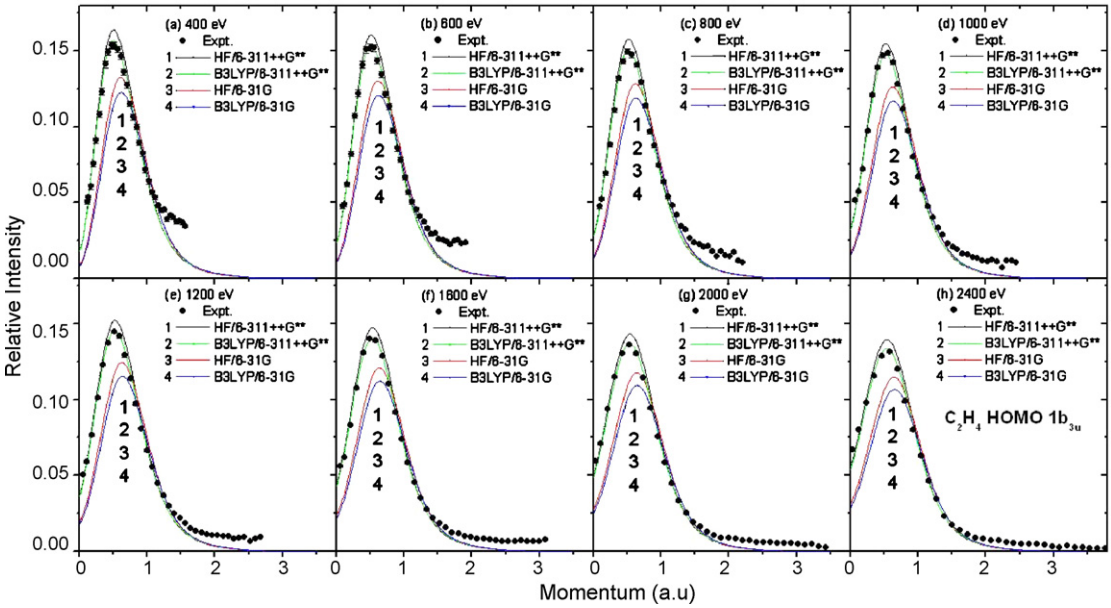

Fig. 3. The experimental orbital electron momentum profiles for the $1b_{3u}$ HOMO orbital of ethylene at different impact energies from 400 eV to 2400 eV compared with the theoretical calculations using DFT and HF methods in PWIA.

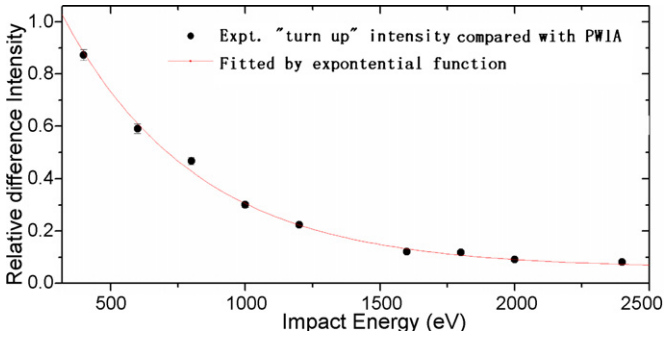

Fig. 4. The intensity differences between experiments and calculations of the HOMO orbital of ethylene as a function of impact energy.

wave function distortions become smaller. Similar effects were also observed in s-like orbitals, see for example the 8a′ orbital of $CHClF_2$ shown in Fig. 5.

Recently, some unexpected discrepancies between experiment and PWIA results were also observed in the low momentum region for the momentum distributions of atomic d orbitals [24] and molecular d-like or π* orbitals [5,8]. For atomic d orbital, the experimental electron momentum distributions can be well reproduced using the DWIA approximation instead of PWIA [24]. As an analogy, it is rational to ascribe the effect observed in the molecular system to the distorted wave effects, and this explanation can qualitatively predict the trend of turn up as the impact energy varies. Unfortunately, the distorted wave calculations are difficult for most of molecular systems due to the multi-center nature of the target. So it is very important to systematically investigate this effect by varying the impact energies. The $1b_{3g}$ orbital of C_2H_4 [5] and the HOMO orbital of O_2 [8] are typical examples of π* orbitals to study the distortion effects in low momentum region. These results could be an experimental test-bed for further calculations in the molecular system. The $1b_{3g}$ orbital of C_2H_4 can be well resolved in the EMS binding energy spectra. Fig. 6 presents the experimental electron momentum distributions and the theoretical calculations of the $1b_{3g}$ orbital at several impact electron energies [5]. It is strange to see that the turn up effects occur in the region of low p since its contribution is normally considered to be dominant at large r, i.e., far from the nuclei. However, as shown in Fig. 7, the $1b_{3g}$ orbital of C_2H_4 is a π* orbital and the low momentum region may correspond to small r according to Brion's explanation [24]. The explanation is quite straightforward: the momentum p is related to the gradient of the wave function in the r space, and for a d-like orbital, the gradient in a given direction is close to zero in the near nuclear region, thus there are distorted wave effects at low momentum [24]. The observed turn up effects of the $1b_{3g}$ orbital become smaller as the impact energy increases. This is further confirmed by the HOMO orbitals of O_2, which is a π* orbital [8]. However, since p is a vector which has three components, a component of p close to zero does not imply that p is close to zero. Actually, the angular momentum L for an atom is a good quantum number, and $L = r \times p$, so the nearer to the nuclear region, the bigger the momentum. Moreover, the momentum operator transforms in the coordinate space and cannot directly generate the intensity distributions. Although it is very likely that the turn up is still the result of the distorted wave effects as Brion suggested, however, possibilities of other effects cannot be excluded totally at current stage. For example, the effects may be due to some other dynamic interaction, such as the dynamic correlation [25,26]. It is well-known that the correlation usually manifests more remarkably at low energy and large r (low momentum) region. As the pioneering EMS works on water [27] and many

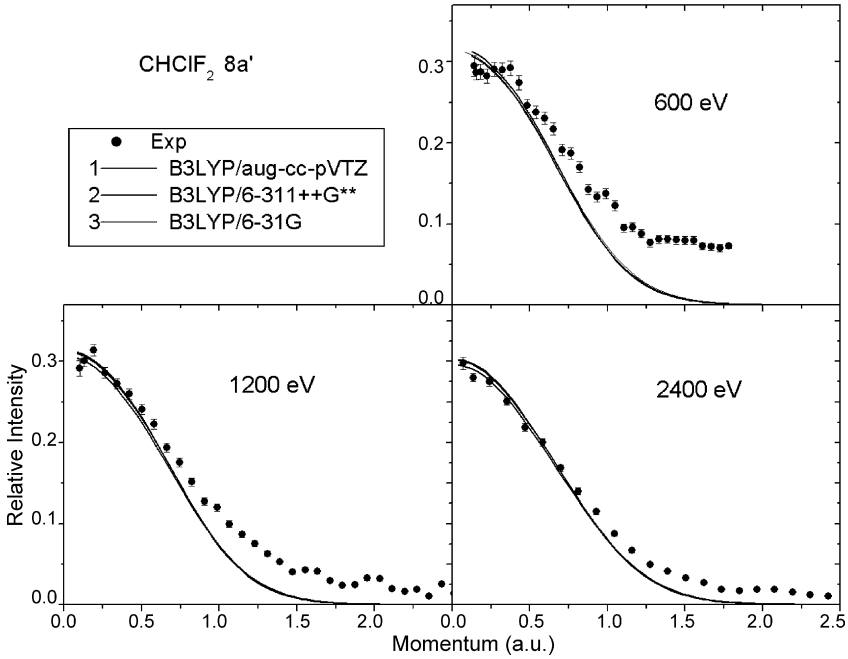

Fig. 5. Momentum distributions of orbital 8a′ of $CHClF_2$ at impact energy of 600 eV, 1200 eV and 2400 eV, respectively, together with theoretical orbital momentum profiles.

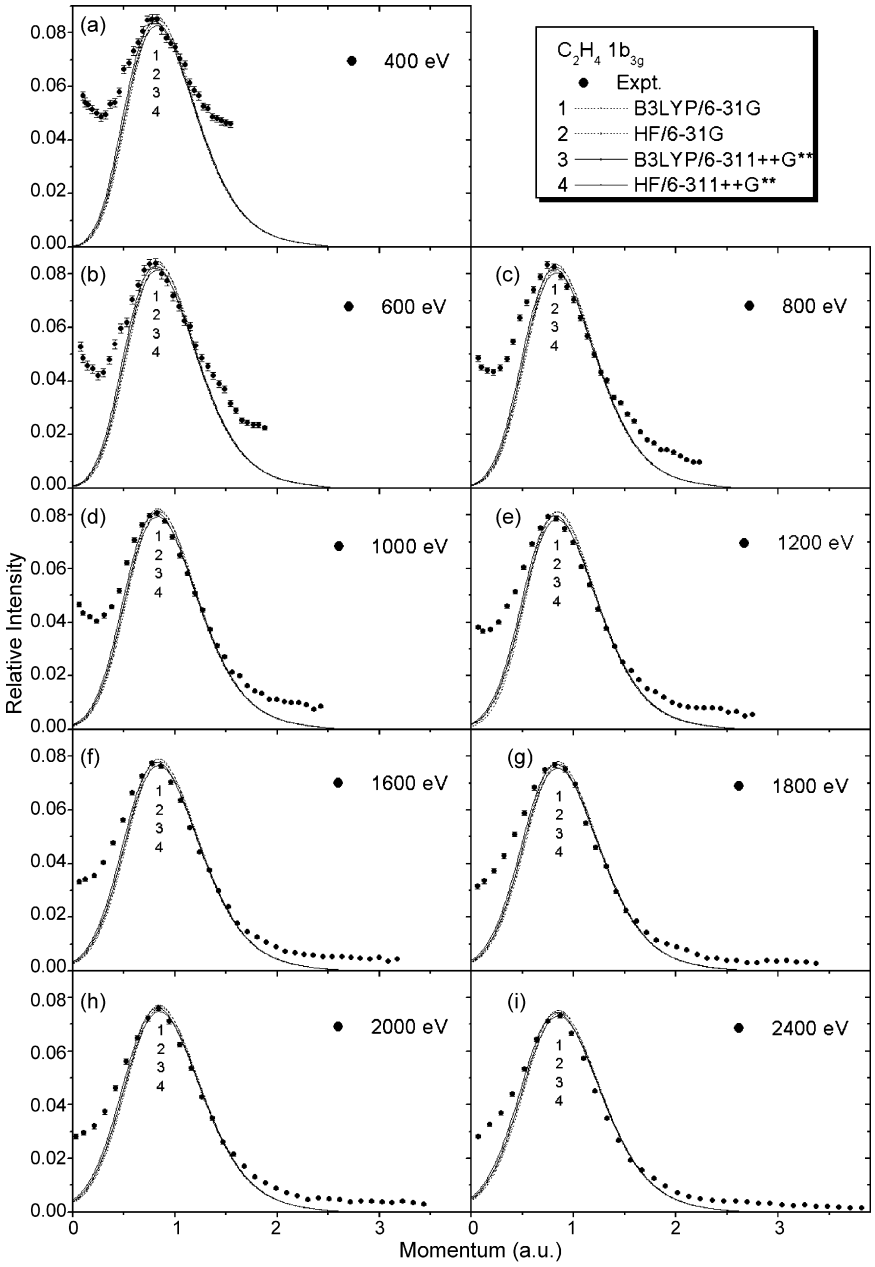

Fig. 6. The experimental orbital electron momentum distributions for the $1b_{3g}$ of ethylene at impact energies from 400 eV to 2400 eV compared with the theoretical calculations using DFT and Hartree–Fock methods in PWIA.

other works of Brion and his collaborators (see papers in [28]) have shown, the main differences between configuration interaction (CI) and HF calculation are located in the low momentum region. Moreover, the nuclear potential is dominant in the region near to the nucleus, thus correlation can only manifest remarkably at large *r*. As a matter of fact, generally, HF calculations can well describe the experimental MD of the inner valence orbitals, but no the MD of outer valence orbitals. It should also be noted that correlations effects are more easily observed in low incident energy experiments than in the high energy ones and that the introduction of correlated wave functions in the calculations does not produce yet a satisfactory agreement between theory and experimental results. The accurate theoretical calculations for the unexpected turn up effects at low momentum are expected to further disclose the nature behind this phenomenon.

4. EMS studies of core orbitals and chemical shift

Core orbitals are essentially localized [29]. They usually have approximate atom-localized electronic states such that the electronic structure of specific elements can be studied even in the presence of many other elements. Binding energies and orbital wave functions of the electrons are element specific in the core region [30]. The chemical shift of core level binding energies makes it possible to differentiate atoms of the same element

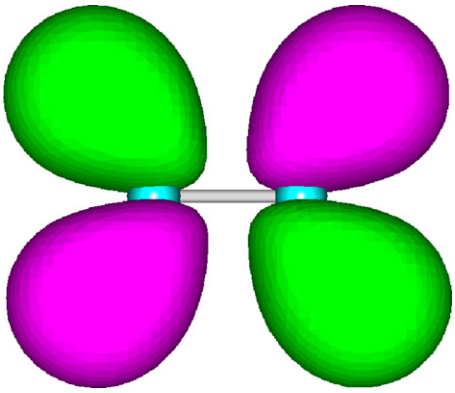

Fig. 7. Contour plot for the ethylene $1b_{3g}$ orbital in position space.

located at the non-equivalent sites in a molecule, producing simpler and more novel picture of the molecular structures [31]. Local characters of the core orbitals also imply that one can find relationships between the chemical shift and chemical properties with site dependence [29]. A good example is the discovery of the chemical shift of S atoms in thiosulfate [32].

Although EMS is a powerful and informative experimental tool to study valence shell orbitals [1–3], EMS has been rarely used to study core orbitals of molecules due to experimental difficulties such as the weakness of the (e, 2e) cross-sections in the core region [33] except for very few species [31]. The study of chemical shift of core orbitals has been dominated by theoretical modeling [30] and has never been studied by EMS. Recently, the EMS study of the two N 1s core orbitals and chemical shift of N_2O, and the four C 1s core orbitals and chemical shift of trifluoroethylacetate ($C_4H_5O_2F_3$, TFEA) were carried out, respectively.

The two nitrogen atoms in N_2O and the four carbon atoms in TFEA are non-equivalent. The N 1s core orbitals (2σ and 3σ) binding energy spectra at $\phi = 12^\circ$ angle and the four C 1s core orbitals (MO1–MO4) binding energy spectra at $\phi = 1^\circ$ angle are shown in Figs. 8 and 9, respectively. Figs. 8 and 9 clearly indicate the chemical shift in binding energies for the N 1s and C 1s core orbitals observed in EMS.

The experimental momentum profiles of the N 1s core orbitals of N_2O have been extracted by deconvolution of binding energy spectra sequentially obtained and angularly correlated. To simulate the momentum distribution, we mapped the core orbitals obtained by the calculation [9] using the extended hybrid functional combined with Lee–Yang–Parr correlation functional (X3LYP) with triple zeta valence basis sets with polarization (TZVP), as shown in Fig. 10 to momentum space. It should be noted that the experimental momentum profiles of the 2σ and 3σ core orbitals have been normalized to the maximum of the calculated momentum distributions, so as to diminish effects of relaxation of the core hole state and screening in the independent-particle model employed in the simulations.

Our experiment confirms the chemical shift predicted in Ref. [34], and s-electron contributions dominate both N 1s core orbitals in N_2O. In Fig. 10 the agreement between the measured and simulated orbital electron momentum distributions for both 3σ and 2σ core orbitals indicates that the approximations such as PWIA and independent-particle approximations are satisfactory not only in the valence [35,36], but also in the core orbitals.

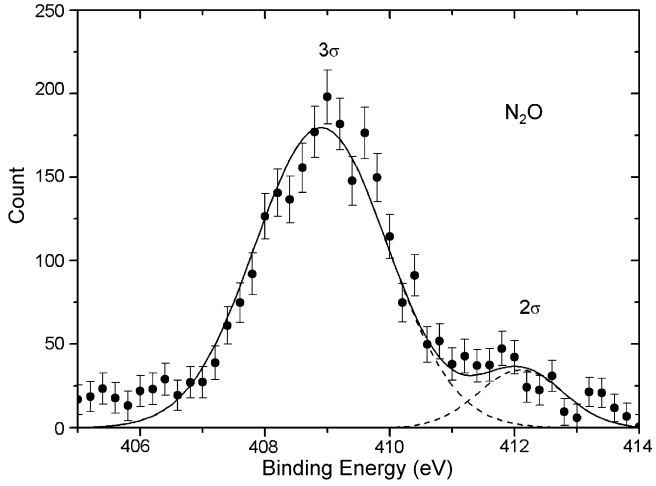

Fig. 8. Binding energy spectra of N_2O at impact energy of 1600 eV and $\phi = 12^\circ$, the dashed and solid lines represent individual and total Gaussian fits to the experimental data, respectively.

The simulated orbital electron momentum distributions indicate that the apparently more localized core orbitals in real space result in much more diffuse orbital electron momentum distributions in reciprocal space (i.e., momentum space). The core orbital electron momentum distributions simulated with B3LYP/TZVP and X3LYP/TZVP models are essentially equivalent in this case. Also, by studying the ratio of 3σ:2σ area cross-section as a function of the azimuthal angle, we find the differences of 3σ and 2σ core orbital electron momentum distributions [9]. Therefore the chemical shift of the N 1s core

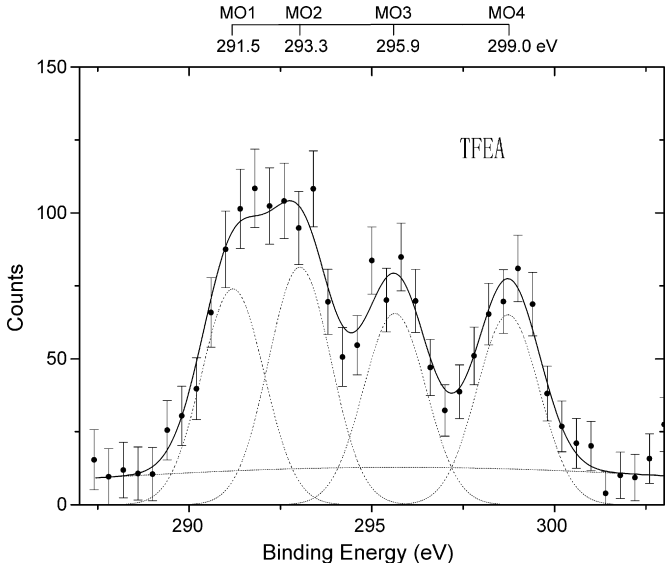

Fig. 9. Binding energy spectra of TFEA at impact energy of 2200 eV and $\phi = 1^\circ$, the dashed and solid lines represent individual and total Gaussian fits, respectively.

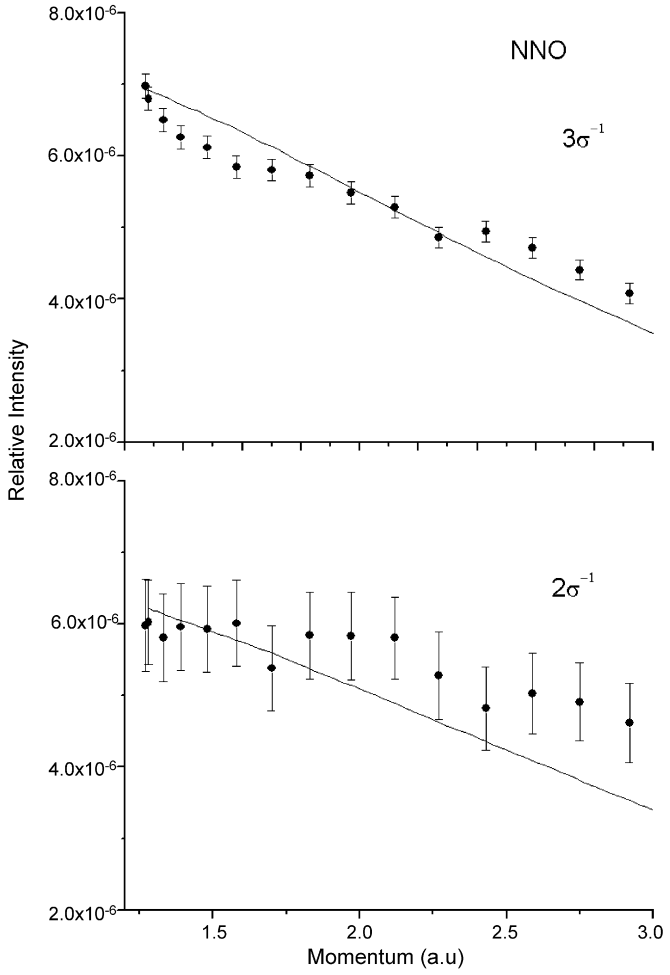

Fig. 10. Theoretical and experimental profiles of momentum of the 2σ and 3σ orbitals of N_2O. Both the calculations for 2σ and 3σ orbitals are modeled with X3LYP/TZVP.

orbitals of N_2O have been observed both in the binding energy spectra and the corresponding electron momentum distributions in EMS. It demonstrates that EMS is capable of observing the chemical shift of the binding energy and the corresponding differences of wave functions, the heart and soul of quantum chemistry.

5. Summary

In summary, the structure and the performances of the newly developed high sensitivity and high resolution electron momentum spectrometer with simultaneous detection in energy and momentum are presented. By comparing the experimental and theoretical momentum distributions of the orbitals with different impact energies, the distorted wave effects are investigated. The results indicate that accurate theoretical calculations are needed to explain the distorted wave effects. Also, the chemical shift and core orbitals of molecules are studied and we found that EMS is capable to observe both the chemical shift of the binding energy of non-equivalent atoms in a molecule and the corresponding differences of wave functions.

Acknowledgements

Authors greatly appreciate the valuable suggestions from Professor C.E. Brion on chemical applications of EMS. Project 10575062 supported by National Natural Science Foundation of China and 20050003084 supported by Specialized Research Fund for the Doctoral Program of Higher Education. Finally, the efforts from Professor X.J. Chen for the early development of the spectrometer at Tsinghua University are appreciated.

References

[1] I.E. McCarthy, E. Weigold, Rep. Prog. Phys. 91 (1991) 789, and references therein.
[2] C.E. Brion, Physics of electronic and atomic collisions, in: T. Andersen, et al. (Eds.), AIP Conference Proceedings, vol. 295, New York, 1993, p. 350, and references therein.
[3] E. Weigold, I.E. McCarthy, Electron Momentum Spectroscopy, Kluwer Academic/Plenum Publishers, New York, 1999.
[4] D.L. Cooper, N.L. Allan, J. Am. Chem. Soc. 114 (1992) 4773.
[5] X.G. Ren, C.G. Ning, J.K. Deng, S.F. Zhang, G.L. Su, F. Huang, G.Q. Li, Phys. Rev. Lett. 94 (2005) 163201.
[6] X.G. Ren, C.G. Ning, J.K. Deng, S.F. Zhang, G.L. Su, F. Huang, G.Q. Li, Rev. Sci. Instrum. 76 (2005) 063103.
[7] X.G. Ren, C.G. Ning, J.K. Deng, S.F. Zhang, G.L. Su, Y.R. Huang, G.Q. Li, J. Electron Spectrosc. Relat. Phenom. 151 (2006) 92.
[8] C.G. Ning, X.G. Ren, J.K. Deng, G.L. Su, S.F. Zhang, G.Q. Li, Phys. Rev. A 73 (2006) 027704.
[9] G.L. Su, C.G. Ning, J.K. Deng, X.G. Ren, S.F. Zhang, Y.R. Huang, T.C. Yang, F. Wang, Chem. Phys. Lett. 422 (2006) 308.
[10] C.G. Ning, J.K. Deng, G.L. Su, H. Zhou, X.G. Ren, Rev. Sci. Instrum. 75 (2004) 3062.
[11] J.K. Deng, G.Q. Li, Y. He, J.D. Huang, H. Deng, X.D. Wang, F. Wang, Y.A. Zhang, C.G. Ning, N.F. Gao, Y. Wang, X.J. Chen, Y. Zheng, J. Chem. Phys. 114 (2001) 882.
[12] G.L. Su, C.G. Ning, S.F. Zhang, X.G. Ren, H. Zhou, B. Li, F. Huang, G.Q. Li, J.K. Deng, Y. Wang, Chem. Phys. Lett. 390 (2004) 162.
[13] X.G. Ren, C.G. Ning, J.K. Deng, S.F. Zhang, G.L. Su, F. Huang, G.Q. Li, Chem. Phys. Lett. 404 (2005) 279.
[14] C.G. Ning, X.G. Ren, J.K. Deng, G.L. Su, S.F. Zhang, S. Knippenberg, M.S. Deleuze, Chem. Phys. Lett. 421 (2006) 52.
[15] C.G. Ning, X.G. Ren, J.K. Deng, S.F. Zhang, G.L. Su, F. Huang, G.Q. Li, Chem. Phys. Lett. 407 (2005) 423.
[16] X.G. Ren, C.G. Ning, J.K. Deng, G.L. Su, S.F. Zhang, Y.R. Huang, Phys. Rev. A 73 (2006) 042714.
[17] X.G. Ren, C.G. Ning, J.K. Deng, G.L. Su, S.F. Zhang, Y.R. Huang, G.Q. Li, Phys. Rev. A 72 (2005) 042718.
[18] C.G. Ning, X.G. Ren, J.K. Deng, S.F. Zhang, G.L. Su, H. Zhou, B. Li, F. Huang, G.Q. Li, Chem. Phys. Lett. 402 (2005) 175.
[19] C.G. Ning, X.G. Ren, J.K. Deng, S.F. Zhang, G.L. Su, H. Zhou, B. Li, F. Huang, G.Q. Li, J. Chem. Phys. 122 (2005) 224302.
[20] T.C. Yang, C.G. Ning, G.L. Su, J.K. Deng, S.F. Zhang, X.G. Ren, Y.R. Huang, Chin. Phys. Lett. 23 (2006) 1157.
[21] S.F. Zhang, C.G. Ning, J.K. Deng, X.G. Ren, G.L. Su, T.C. Yang, Y.R. Huang, Chin. Phys. Lett. 23 (2006) 583.
[22] C.G. Ning, X.G. Ren, J.K. Deng, G.L. Su, S.F. Zhang, F. Huang, G.Q. Li, Chin. Phys. 14 (2005) 2467.
[23] J.N. Migdall, M.A. Coplan, D.S. Hench, J.H. Moore, J.A. Tossell, V.H. Smith Jr., J.W. Liu, Chem. Phys. 57 (1981) 141.
[24] C.E. Brion, Y. Zheng, J. Rolke, J.J. Neville, I.E. McCarthy, J. Wang, J. Phys. B 31 (1998) L223.
[25] S.J. Desjardins, A.O. Bawagan, Z.F. Liu, K.H. Tan, Y. Wang, E.R. Davidson, J. Chem. Phys. 102 (1995) 6385.
[26] X.J. Liu, L.F. Zhu, Z.S. Yuan, W.B. Li, H.D. Cheng, Y.P. Huang, Z.P. Zhang, K.Z. Xu, Phys. Rev. Lett. 91 (2003) 193203.

[27] A.O. Bawagan, C.E. Brion, E.R. Davidson, D. Feller, Chem. Phys. 113 (1987) 19.
[28] A. Hitchcock, T. Leung, J. Electron Spectrosc. Relat. Phenom. 123 (2002) 103.
[29] S. Svensson, J. Phys. B: At. Mol. Opt. Phys. 38 (2005) S821.
[30] F. Wang, J. Mol. Struct. (Theochem) 728 (2005) 31.
[31] S.M. Bharathi, A.M. Grisogono, A. Lahmam-Bennaani, R. Pascual, E. Weigold, J. Electron Spectrosc. Relat. Phenom. 53 (1991) 271.
[32] S. Hagström, C. Nording, K. Siegbahn, Z. Phys. 178 (1964) 439.
[33] U. Amaldi, C. Ciofi degli Atti, Nuovo Cim. A 66 (1970) 129.
[34] F. Wang, F.P. Larkins, M.J. Brunger, M.T. Michalewicz, D.A. Winkler, Spectrochim. Acta A 57 (2001) 9.
[35] Y. Khajuria, M. Takahashi, Y. Udagawa, J. Electron Spectrosc. Relat. Phenom. 134 (2004) 207.
[36] F. Wang, M.J. Brunger, F.P. Larkins, J. Phys. Chem. A 105 (2001) 1254.